JCSE The Journal of Corrosion Science and Engineering
ISSN 1466-8858 Volume 15, Preprint 44 submitted 28 November 2012

Kinetic-thermodynamic studies of substituted mono- and bis- azo dyes as corrosion inhibitors for iron in nitric acid and sodium hydroxide solutions

Loutfy H. Madkour* and U.A. Zinhome**

** Chemistry Department, Faculty of Science and Arts, Baljarashi, Al-Baha University, P.O. Box. (1988), Al-Baha, Kingdom of Saudi Arabia.*
E-mail: loutfy.madkour@yahoo.com

***Chemistry Department, Faculty of Science, Tanta University, 31527, Tanta, Egypt.*

ABSTRACT

This investigation is designed to apply an advanced kinetic-thermodynamic model on the experimental data obtained from acidic and alkaline corrosion of iron using mono- and bis-azo dyes as corrosion inhibitors. The inhibition properties of the tested azo dyes on corrosion of iron in HNO_3 and NaOH media were analyzed by gravimetric, thermometric and polarization measurements. The three studied methods gave consistent results. Polarization study showed that all the inhibitors are mixed type in acidic, act mainly as cathodic in alkaline solution. The synthesized azo dye derivatives exhibit good inhibition properties, obeys the Frumkin adsorption isotherm. The large values of the change in the standard free energy of adsorption (ΔG^{o}_{ads}), equilibrium constant (K_{ads}) and binding constant (K_b) revealed that the reactions proceed spontaneously and result in highly efficient physisorption mechanism and stronger electrical interaction between the double layer existing at the phase boundary and the adsorbing molecules. The inhibition efficiency depends on the number of adsorption oxygen sites (OH and OMe groups), their charge density and π-electron clouds. The inhibition efficiency evaluated via theoretical methods was well accorded with reported experimental ones, following the same order as: *α*-naphthyl- ligand > *β*-naphthyl > *p*-anisdine > *p*-toluidine > *o*-toluidine > *m*-toluidine derivative. This research might provide a theoretical inhibition performance evaluation approach for homologous inhibitors.

Keywords: Corrosion, inhibitor, mono- and bis- azo dyes, iron, HNO_3, NaOH

JCSE The Journal of Corrosion Science and Engineering
ISSN 1466-8858 Volume 15, Preprint 44 submitted 28 November 2012
*Corresponding author. Tel.: +966 0568219461 (*Saudi Arabia*)

1. Introduction

Among numerous anticorrosion measures, corrosion inhibitor is widely used and acts as one of the most economical and effective ways [1-3]. A number of organic compounds [4-7] are known to be applicable as corrosion inhibitors for iron and its alloys in acidic environments. Such compounds contain nitrogen, oxygen or sulphur in a conjugated system can donate one pair of electrons, and multiple bonds, and function via adsorption of the molecules on the metal surface, creating barrier against corrosion attack [8-14]. The adsorption bond strength depends on the composition of the metal and corroding inhibitor structure and concentration as well as temperature. The corrosion inhibition of iron in 2.0 M HNO_3 and 2.0 M NaOH solutions has been reported recently by using Schiff bases [15]. Generally, localized corrosion can be prevented by the action of adsorptive inhibitors which prevent the adsorption of the aggressive anions or by the formation of oxide films on the metal surface [15-22]. It has been observed that the adsorption of these inhibitors depends on the physico-chemical properties of the functional groups and the electron density at the donor atom. The adsorption occurs due to the interaction of the lone pair and/or π-orbitals of inhibitor with d- orbitals of the metal surface atoms, in which the metal acts as an electrophile and the inhibitor acts as a Lewis base whose nucleophilic centers are O and/or N atoms with free electronic pairs which are readily available for sharing, which evokes a greater adsorption of the inhibitor molecules onto the surface, leading to the formation of a corrosion protection film [15, 20-25]. Furthermore, adsorption and consequently the efficiency of an inhibitor do not only depend on its structure, but also on the characteristics of

ISSN 1466-8858 Volume 15, Preprint 44 submitted 28 November 2012

the environment in which it acts, the nature structure , the charge of metal surface and other experimental conditions [26]. The choice of effective inhibitors is based on their mechanism of action and electron-donating ability. The significant criteria involved in this selection are molecular structure, electron density on the donor atoms, solubility and dispersibility [27-30]. In any case, adsorption is general over the metal surface and the resulting adsorption layer function as a barrier, isolating the metal from the corrosion [31]. The inhibition efficiency has found to be closely related to inhibitor adsorption abilities and molecular properties for different kinds of organic compounds [32]. Previously, some work has been done in our laboratory on these bis-and mono-azo dyes whereas; the compounds are successful as corrosion inhibitors on aluminum and zinc metals in hydrochloric acid and sodium hydroxide [33]. The choice of these (MAD) and (BAD) as inhibitors is based on the following considerations: these molecules (a) can be easily synthesized from relatively cheap materials, (b) –N=N- group, electronegative oxygen and aromatic rings as active centers (c) and have high solubility in acidic and alkaline media. The action of such investigated (MAD) and (BAD) inhibitors depend on the specific interaction between the functional groups and the metal surface. The present study was undertaken to investigate the inhibition of iron corrosion in 2.0 M HNO_3 and NaOH by these two newly synthesized series (MAD) and (BAD) derivatives. The study was conducted by using weight loss, thermometric, electrochemical polarization measurements and confirmed by using kinetic and thermodynamic calculations.

2. Materials and Methods

2.1. Synthesis of mono-and bis-azo dye (MAD) and (BAD) inhibitors

The investigated azo dye derivatives were synthesized by diazotization of

ISSN 1466-8858 Volume 15, Preprint 44 submitted 28 November 2012

primary aromatic amines and coupling with the corresponding naphthol derivatives in the ratio 1:1 and 2:1 in the case of (MAD) and (BAD) respectively. The compounds are purified and characterized by ^{1}H NMR, IR spectroscopy and element analysis before use [33]. The inhibitor solutions were prepared by dissolving the appropriate amount in 10 cm^3 Analar ethanol. The desired volume of the free inhibitor was added to the electrolyte solution. The ratio of ethanol was kept constant for each test. This stock solution was used for all experimental purposes.

The molecular structure of (MAD) and (BAD) is given below:

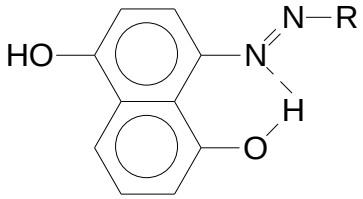

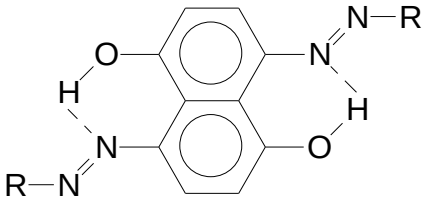

R		R	
α- Naphthyl	(**1**)	α- Naphthyl	(**7**)
β- Naphthyl	(**2**)	β- Naphthyl	(**8**)
C_6H_4OMe-*p*	(**3**)	C_6H_4OMe-*p*	(**9**)
C_6H_4Me-*p*	(**4**)	C_6H_4Me-*p*	(**10**)
C_6H_4Me-*o*	(**5**)	C_6H_4Me-*o*	(**11**)
C_6H_4Me-*m*	(**6**)		

It is evident that (MAD) and (BAD) are aromatic compounds containing nitrogen and oxygen atoms, which could easily be protonated in acidic solution, and several π-electrons exist in these molecules.

2.2. Electrodes and electrolytes

The corrosion tests were performed on a freshly prepared iron specimens of the following composition (in wt.%): 0.091% C, 0.002% Si, 0.196% Mn, 0.011% P, 0.016% S, 0.009% Cr, 0.021% Ni, 0.01% Al, 0.024% Cu and Fe balance. The test specimens used in the weight loss measurements were mechanically cut into (2.0 cm x 2.0 cm x 0.1 cm) dimensions, for thermometric study, specimens were cut into (10.0 cm x 1.0 cm x 0.1 cm) sizes and for electrochemical study, specimens was soldered with Cu-wire for electrical connection and mounted into the epoxy resin to offer only one active flat surface exposed to the corrosive environment. Before each experiment, the electrode was first mechanically abraded with a sequence of emery papers of different grades (320, 400, 800, 1000, and 1200), respectively, followed by washing with double distilled water and finally degreased in absolute ethanol and acetone, dried in room temperature and stored in a moisture free desiccators before their use in corrosion studies [15,20,22,33-36]. The corrosive solutions, 2.0 M HNO_3 and 2.0 M NaOH were prepared by dilution of analytical grade reagents with double distilled water. The concentration range of employed inhibitors was (5 x 10^{-4} to 0.1 mM) in 2.0 M HNO_3 and 2.0 M NaOH.

2.3. Measurements

Three methods weight loss assessment, thermometric, and electrochemical polarization curves were used to determine the corrosion inhibition efficiencies of (MAD) and (BAD) for iron corrosion in acidic and alkaline solution.

2.3.1. Weight loss measurements

Weight loss experiments were done according to the standard methods as reported in literature. The corrosion rates, C_R (mg cm^{-2} h^{-1}) were calculated according to the following equation [37]:

$$CR = W/Dta \quad (1)$$

where W is the average weight loss of three parallel iron sheets (one specimen in each beaker), a is the total surface area of the iron specimen, t is the immersion time and D is the density of iron specimen. The inhibition efficiency (In%) was calculated using the following equation [38]:

$$In\% = [(C_{R\ (uninh)}) - C_{R(inh)}) / C_{R(uninh)}] \times 100 \qquad (2)$$

where $C_{R(uninh)}$ and $C_{R(inh)}$ are the values of corrosion rates (mg cm^{-2} h^{-1}) obtained of iron in uninhibited inhibited solutions, respectively.

Weight loss measurements were conducted under total immersion using 250 mL capacity beakers containing 200 mL test solution at 303 K maintained in a thermo stated water bath. The iron specimens were weighed accurately (using Mettler AG104 0.1 mg Analytical Balance) and suspended in the beaker with the help of rod and hook. The specimens were immersed in 250 mL beaker contained 200 mL 2.0 M HNO_3 and/or 2.0 M NaOH with and without addition of different concentrations (5×10^{-7} – 1×10^{-4} M) of the tested inhibitors. After different immersion time intervals of (0.5, 1.0, 1.5, 2.0, 2.5, 3.0, 3.5, 4.0, 4.5, 5.0, 5.5 and 6.0 h), the iron specimens were taken out, washed, dried, and weighed accurately. The average weight loss tests at a certain time were repeated for each of the three pieces of iron specimens. The specimens were immersed in the solutions without blocking any side, and the whole specimen area was considered in the calculation.

2.3.2. Thermometric measurements

The reaction vessel used was basically the same as that described by Mylius [39]. An iron piece specimens were cut into (10.0 cm x 1.0 cm x 0.1 cm) sizes were immersed in 30 cm^3 of 2M HNO_3 and/or 2M NaOH in the absence and presence of inhibitors respectively. The temperature of the system was followed

as a function of time. The reaction number (*RN*) and the reduction in reaction number (% red *RN*) were calculated using the following Eqs. (3) and (4):

$$RN = (T_{max} - T_i)/t \quad (3)$$

$$\%\ \text{red}\ RN = [(RN_{(uninh)} - RN_{(inh)}/\ RN_{(uninh)}] \times 100 \quad (4)$$

where T_{max} and T_i, are the maximum and initial temperatures, respectively, t is the immersion time (in minutes) required to reach T_{max}. , $RN_{(uninh)}$ and $RN_{(inh)}$ are the reaction number in the absence and presence of inhibitors, respectively [15,20,33,40]. The specimens were immersed in the solutions without blocking any side.

2.3.3. Polarization measurements

Potentiostatic polarization experiments were carried out using a standard electrochemical three-electrode cell [15, 20, 22, 33, 34]. Iron acts as working electrode (WE), saturated calomel electrode (SCE) as reference electrode and platinum was used as counter electrode, which was separated from the main cell compartment by a glass sinter and an iron rod working electrode with a fine lugging capillary placed close to the working electrode to minimize ohm resistance. In order to avoid contamination, the reference electrode was connected to the working-electrode through a salt bridge filled with the test solution. The tip of the bridge was pressed against the working electrode in order to compensate the ohmic drop. In deaerated electrochemical tests, the solution under investigation was 25 cm^3 deoxygenated with nitrogen of high purity before tests for 4 h while the flow of the gas in the solution was continued during the measurements. The bubbling rate, which was not measured, was small and the same which could be ignored in all the experiments. Measurements were performed on a planar disk electrode (A= 1cm^2). The edges of the working electrode were masked by appropriate resins (Duracryle, Spofa-Dental, and Praha). The electrodes were rinsed in an ultrasonic bath containing

ISSN 1466-8858 Volume 15, Preprint 44 submitted 28 November 2012

double distilled water before being immersed in the cell. The polarization measurements were carried out using a laboratory potentiostat (Wenking Potentioscan model POS 73, Germany). In this method, the working electrode was immersed in test solution for 45 min until the open circuit potential was reached. After that the working electrode was polarized in both cathodic and anodic directions. The obtained values of (current-potential) were fitted, and the polarization curves were then plotted. The values of corrosion current density (i_{Corr}) were calculated from the extrapolation of straight part of the Tafel lines. The potential increased with respect to the open circuit potential vs.corrosion potential (E_{Corr}). The inhibition efficiency (*In %*) was defined as:

$$In\% = [(i_{Corr(uninh)} - i_{Corr(inh)}) / i_{Corr(uninh)}] \times 100 \quad (5)$$

where $i_{Corr(uninh)}$ and $i_{Corr(inh)}$ are the corrosion current density values without and with inhibitors . The cell temperature was kept constant at 303.0 ± l.0 K in an ultra-thermostat.

3. Results and discussion

Corrosion inhibition performance of the synthesized inhibitors can be evaluated using electrochemical and chemical techniques.

3.1. Structure of mono- and bis- azo dyes

The chemical structures of the synthesized inhibitors (MAD) and (BAD) were confirmed using ^{1}H NMR, IR spectroscopy and elemental analysis. The molecular structures of the studied (MAD) and (BAD) derivatives are illustrated in the following Schemes 1 and 2, respectively:

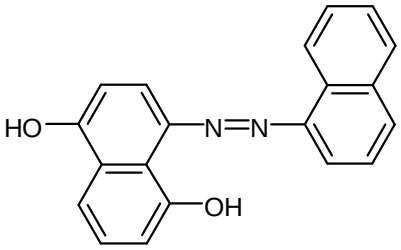

Mono-α-naphthyl amine (**1**)

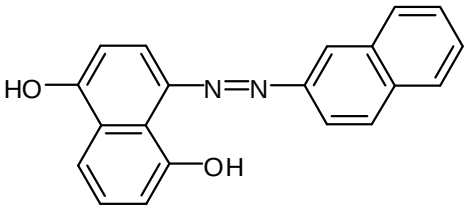

Mono-β -naphthyl amine (**2**)

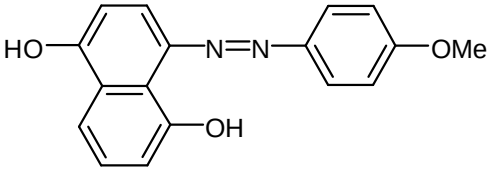

Mono-p-anisidine (**3**)

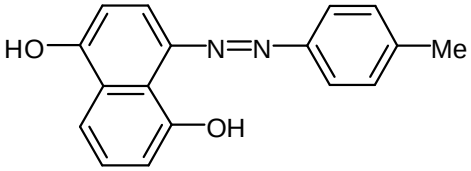

Mono-p-toluidine (**4**)

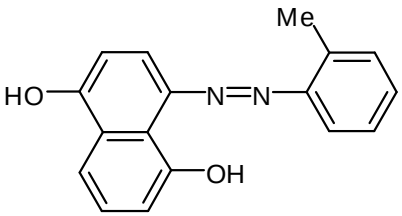

Mono-o-toluidine (**5**)

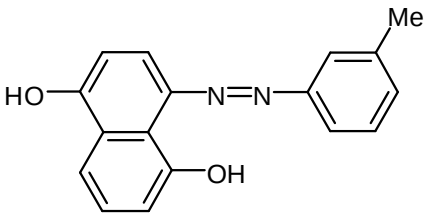

Mono-m-toluidine (**6**)

Scheme1. Molecular structures of the studied synthesized mono- azo dye derivatives.

JCSE The Journal of Corrosion Science and Engineering
ISSN 1466-8858 Volume 15, Preprint 44 submitted 28 November 2012

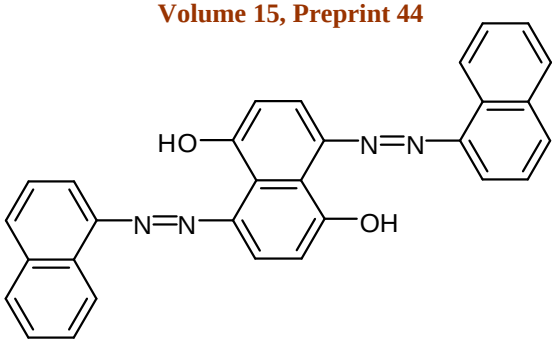

Bis-α-naphthyl amine (**7**)

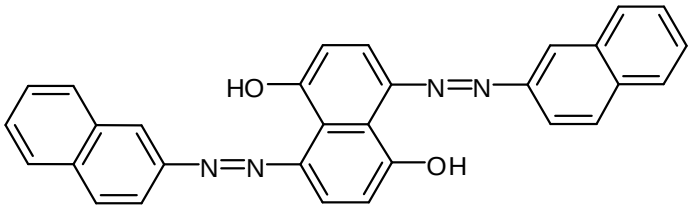

Bis-β -naphthyl amine (**8**)

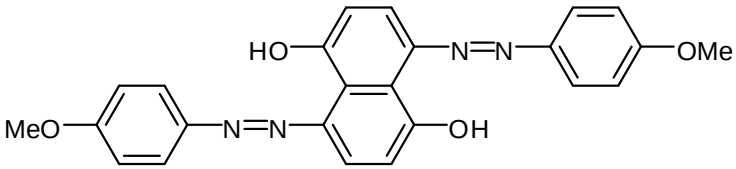

Bis-p-anisidine (**9**)

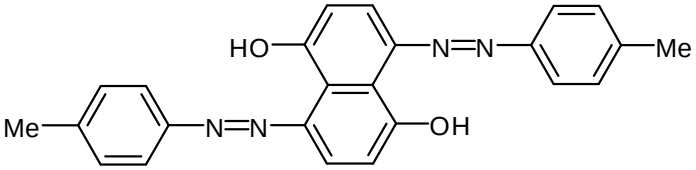

Bis-p-toluidine (**10**)

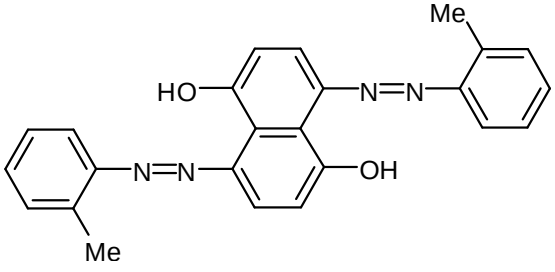

Bis-o-toluidine (**11**)

ISSN 1466-8858 Volume 15, Preprint 44 submitted 28 November 2012

Scheme2. Molecular structures of the studied synthesized bis- azo dye derivatives.

3.1. Weight loss measurements

Gravimetric evaluation of the synthesized inhibitors and the effect of inhibitor dose, for the chemical methods, a weight loss measurement are ideally suited for long term immersion test. Corroborative results between weight loss and other techniques have been reported [41-43]. At present, weight loss is probably the most widely used method of inhibition assessment [15, 35-36, 44-48]. It is the most accurate and precise method for determining metal corrosion rate because the experimentation is easy to replicate and, although long exposure times may be involved, the relatively simple procedure reduces the propensity to introduce systematic errors. The anodic dissolution of iron in acidic media and the corresponding cathodic reaction has been reported to proceed as follows [49]:

$$Fe \rightarrow Fe^{2+} + 2e^{-} \quad (6)$$

$$2\,H^{+} + 2e^{-} \rightarrow 2\,H_{ads} \rightarrow H_2 \quad (7)$$

As a result of these reactions, including the high solubility of the corrosion products, the metal loses weight in the solution. The effect of addition of different (MAD) and (BAD) derivatives at various concentrations on the iron corrosion in 2.0 M HNO_3 and 2.0 M NaOH solution was studied by weight loss measurements at 303 K. Table 1 represents the corrosion inhibition efficiencies (In%) of the synthesized inhibitors (at 5 $x10^{-7}$ – 1x 10^{-4} M) on the iron corrosion in 2.0 M HNO_3 solution at 303 K. The extent of covering the metal surface by inhibitor molecules can be expressed in terms of the surface coverage (θ) which represents the degree of arrangement of inhibitor molecules on the metal surface [50]:

$$\theta = 1 - (W_i / W_o) \quad (8)$$

ISSN 1466-8858 Volume 15, Preprint 44 submitted 28 November 2012

where W_i and W_o are the weight losses of the iron specimens in presence and absence of inhibitors respectively. It is clear that the gradual increase of the inhibitor dose from 5 x 10^{-7} to 1 x 10^{-4} M increases the adsorbed molecules onto the metal surface, which increases the surface coverage and the inhibition efficiencies of tested inhibitors (Table 1). This effect may be attributed to the accumulation of the inhibitor molecules onto the metal surface, which decreases the interaction between the acidic medium and the metal surface. The adsorption of inhibitor molecules onto the metal surface occurred due to the interaction between the negatively charged centre of the metal surface and the positively charged head groups (N^+), and π-electrons of the inhibitor molecules. It is reported that the heteroatoms facilitate the adsorption of inhibitor molecules at the metal surface due to the electronegativity factor [51, 52]. The inhibition tendency of the corrosion inhibitors is increased in presence of the heteroatoms in the following sequence: S > N > O [53]. The high inhibition tendency of the tested inhibitors may be attributed to the presence of the nitrogen and oxygen atoms in their chemical structure. The nitrogen atoms participated in the azo group is protonated in the acidic medium, which enhances their adsorption onto the metal surface. The maximum inhibition efficiencies were obtained at 1 x 10^{-4} M for (MAD) and (BAD) derivatives at 303 K. From Table 1, it is clear that the order of inhibition efficiency obtained from weight loss measurements of (MAD) and (BAD) is as follows:

α-naphthyl- ligand > β-naphthyl > *p*-anis dine > *p*-toluidine > *o*-toluidine > *m*-toluidine derivative.

It is apparent from the gravimetric data in Table 1 that the gradual increase of the inhibitor dose decreases the corrosion rates. The lowest corrosion rate of iron was obtained at 1 x 10^{-4} M of the synthesized inhibitors. The adsorbed inhibitor molecules at higher doses form a well arranged monolayer on iron metal surface where the organic parts (alkyl chains) are arranged to locate the medium and the

ISSN 1466-8858 Volume 15, Preprint 44 submitted 28 November 2012

head groups attached to the metal surface, that inhibits the metal-acid reaction to large extent [54]. Fig.1 shows corrosion loss of weight-loss measurement as a function of time. Weight-loss in mg cm^{-2} of the iron surface area was determined in an open system under unstirred conditions in 2.0 M HNO_3 and 2.0 M NaOH solution at time intervals. The observed curves in Fig.1 (a) are characterized by a rapid rise at the first hour from immersion, and then the curves are followed by slow rise. The observed corrosion parameters values depend on the nature and concentration of the applied corrosive medium. The observed curves in nitric acid solution (Fig.1 (a)) confirm the pre-immersion oxide film formed on the iron surface gives no protection against nitric acid attack. The weight loss-time curves observed in alkaline medium show a gradual continuously small definite increasing of weight loss as the time of immersion increases, give straight lines starting from the origin (Fig.1 (b)), this is because of the oxide film which originally formed at the electrode surface was easily detectable in NaOH medium. Thus, the dissolution of iron itself in 2.0 M NaOH solution is linearly to the reaction time (at 303 K). This behaviour is an indication of zero order reaction with general equation (Eq. (9)).

$$W_t = kt \qquad (9)$$

Where *Wt* is the weight loss of iron at time *t* and *k* is the rate constant. The values of *k* can be calculated from the slope of the W_t - *t* curves at the given temperature. In this manner *k* of iron dissolution in NaOH and in the presence of the inhibitors were determined. The values of *k* can also be used for comparing the inhibition efficiencies of the inhibitors. It is obvious that the loss in weight in the presence of the investigated (MAD) and (BAD) is lower than that in its absence, and mostly decreases as the concentration of the additives increased from $5 \times 10^{-7} - 1 \times 10^{-4}$ M; consequently, (θ) and (% In) increases as denoted by the decrease in weight loss values. The weight loss-time curves for the tested synthesized azo dye derivatives (Fig.1) fall below that of the free corrosive

ISSN 1466-8858 Volume 15, Preprint 44 submitted 28 November 2012

media. Thus, both (MAD) and (BAD) act as strong inhibitors. The corrosion rate of iron in nitric acid medium is under anodic control [55] which is:

$$Fe + OH^- \leftrightarrow FeOH_{ads} + H^+ + e^- \quad (rds) \qquad (10)$$

$$FeOH_{ads} \rightarrow FeOH^+ + e^- \qquad (11)$$

$$FeOH^+ + H^+ \leftrightarrow Fe^{2+} + H_2O \qquad (12)$$

where 'red' stands for rate-determining step.

The adsorption isotherm experiments were performed to have more insights into the mechanism of corrosion inhibition, since it describes the molecular interaction of the inhibitor molecules with the active sites on the iron surface [56]. The surface coverage, θ, was calculated according to the previous equation (8). The surface coverage values (θ) for different inhibitor concentration were tested by fitting to various isotherms and the models considered were [57]:

$$\text{Temkin isotherm } \exp(f.\,\theta) = k_{ads}.\,C \qquad (13)$$

$$\text{Langmuir isotherm } (\theta/1-\theta) = k_{ads}.\,C \qquad (14)$$

$$\text{Frumkin isotherm } (\theta/1-\theta)\,exp\,(-2f.\,\theta) = k_{ads}.\,C \qquad (15)$$

$$\text{Freundluich isotherm } \theta = k_{ads}.\,C \qquad (16)$$

Where k_{ads} is the equilibrium constant for adsorption process, C is the concentration of inhibitor and f is the energetic inhomogeneity. Attempts were made to fit the θ values to various isotherms including Langmuir, Temkin, Frumkin and Freundluich. By far the best fit is obtained with the Frumkin adsorption isotherm [58]. The plot of (θ) vs. log C gave S-shaped curves as shown in Fig.2. Stabilizing effect [59] that comes from the complex compound formed indicates rearrangement of the charge density inside the molecule, thus shows its corrosion inhibition. This is supported by U.V. spectrophotometer analysis and also conductivity measurements.

3.2. Thermometric measurements

In this method the temperature change of the system involving iron dissolution in 2.0 M HNO_3 was followed without and with different concentrations of the investigated (MAD) and (BAD) derivatives, as given in Fig.3 for compound (**1**) as an example for all additives . An incubation period is first recognized along which the temperature rises gradually with time. The temperature- time curves provide a mean of differentiating between weak and strong adsorption. The thermometric data are depicted in Table 2. It is evident that, the dissolution of iron in 2.0 M HNO_3 starts from the moment of immersion. On increasing the concentration of the inhibitor from (5×10^{-7} – 1×10^{-4} M) the value of T_{max} decreases, whereas the time (t) required reaching T_{max} increases, and both factors cause a large decrease in (RN) and increasing of (% red RN) of the system [39] , as shown in Table 2. This indicates that the studied synthesized azo dye additives retard the dissolution presumably by strongly adsorption onto the metal surface . The extent of inhibition depends on the degree of the surface coverage (θ) of the iron surface with the adsorbate. Iron, as an active element, always carries an air formed oxide, which specifically and very strongly adsorbs H^+ and OH^- ions according to the equations (10 - 12), these reactions takes place along the incubation period. The heat evolved from the above reactions accelerates further dissolution of the oxide and activates the dissolution of the iron metal exposed to the aggressive medium.

The relation between RN, time delay (Δt) and/or log (Δt) versus molar concentration of the additives confirms a two-step adsorption process [60], at first a monolayer of the adsorbed is formed on the iron electrode surface, and then it is followed by the adsorption of a second adsorbed layer or a chemical reaction leading to the deposition of the (azo dye-Fe complex) on the metal surface. The plot of Δt and/or log (Δt) as a function of log C_{In} yields a linear relation shape for the first region of the curve then a region of constancy; this

reveals the completion of the adsorbed monolayer of the inhibitor. In thermometric measurements (% red RN_{In}) values are taken as the measure for the corrosion inhibition efficiency (% In). Plots of % red *RN* versus molar concentration (C_{In}) of the additives for iron corrosion in 2.0 M HNO_3 are invariably sigmoidal in nature as shown in Fig.4. The inhibition efficiency of the synthesized (MAD) and (BAD) derivatives depends on many factors, including the molecular size, heat of hydrogenation, mode of interaction with iron electrode surface, formation of metallic complexes and the charge density on the adsorption sites. Adsorption is expected to take place primarily through functional groups, essentially OH and OCH_3 would depend on its charge density as reported [61]. The thermometric technique is not applied for the dissolution of iron in sodium hydroxide because of the temperature changes of the system involving iron immersed in 2.0 M NaOH solution was varied but with a negligible change. This is due to the fact that the oxide film originally formed on the iron electrode surface is easily detectable in 2.0 M NaOH.

3.3. Tafel polarization curves measurements

Electrochemical measurement is considered to be a fast and efficient method which reflects the transient electrochemical process, so it can be used for measuring corrosion rate on-site, because from the shape of the experimental curve it may be possible to obtain important information on the kinetics of the corrosion reactions. Fig.5 shows Tafel polarization curves of iron in 2.0 M HNO_3 and 2.0 M NaOH in the absence and presence of different concentrations of (MAD) inhibitor (**1**) at 303 K (as an example). As seen from Fig.5 (a) and (b), the anodic and cathodic Tafel slopes are changed in small range and independent on the inhibitors concentrations, indicating that the inhibition role of these inhibitors is not through the interference on the reactions of metal dissolution and reduction of protons. This indicates that the (MAD) and (BAD) derivatives act as adsorptive inhibitors, i.e., they reduce anodic dissolution and also retard

ISSN 1466-8858 Volume 15, Preprint 44 submitted 28 November 2012

the hydrogen evolution reaction [62] via blocking the active reaction sites on the iron surface, or even can screen the covered part of the electrode; and therefore protect it from the action of the corrosion medium [63].

This effect is attributed to the adsorption of the inhibitor on the active sites of the iron surface. The values of corrosion current, corrosion potential, cathodic and anodic Tafel slopes are obtained by the anodic and cathodic regions of the Tafel plots. The corrosion current density (i_{corr}) can be obtained by extrapolating the Tafel lines to the corrosion potential and the inhibition efficiency (%In) values were calculated from Eq.(5). It is obvious that the slopes of the cathodic (βc) Tafel lines almost changed in small values upon addition of the tested azo dye derivatives. The parallel cathodic Tafel lines suggested that the addition of inhibitors to the 2.0 M HNO_3 solution do not modify the hydrogen evolution mechanism and the reduction of H^+ ions at the iron surface which occurs mainly through a charge-transfere mechanism. The shift in the anodic Tafel slope (βa) values may be due to the adsorption of nitrate ions/or inhibitor modules onto the iron surface [64]. It is also clear that there is a shift towards cathodic region in the values of corrosion potential (E_{corr}), from the fact that βc > βa. The extent of adsorption of inhibitor molecules onto the metal surface in term of the surface coverage (θ) was calculated using Eq. (17) [65]:

$$\theta = (i_{Corr(uninh)} - i_{Corr(inh)})/i_{Corr(uninh)} \quad (17)$$

where $i_{Corr(uninh)}$ and $i_{Corr(inh)}$ are the corrosion current densities in the absence and presence of the inhibitors, respectively. It is clear from the polarization curves that the increase of the inhibitor concentrations decreases the corrosion current (i_{Corr}) which consequently increases the surface coverage values. Also, the corrosion current density (i_{Corr}) of iron corrosion reaction is decreased by increasing the inhibitor dose. In this respect, the decrease in current density in presence of the different synthesized inhibitors reveals that the corrosion

ISSN 1466-8858 Volume 15, Preprint 44 submitted 28 November 2012

reaction proceeded much slower than the uninhibited medium. Moreover, the gradual increase in the inhibitor doses considerably decreases the corrosion current densities. Comparing the corrosion currents and the inhibition efficiencies of the used inhibitors shows that increasing the inhibitor doses decreases the corrosion currents, and consequently increases the retardation of the iron dissolution in the acidic and alkaline media. The results show that (MAD) (**1**) and (BAD) (**7**) inhibitors at 1 x 10^{-4} M produce the lowest corrosion current densities (7.713, 7.488 mA cm^{-2}) and the maximum inhibition efficiencies obtained were 77.8% and 78.4% respectively (Table 3). In literature, it has been reported that if the displacement in E_{corr} (i) is > 85 mV with respect to E_{corr}, the inhibitor can be seen as a cathodic or anodic type and (ii) if displacement in E_{corr} is < 85 mV, the inhibitor can be seen as mixed type. In our study the maximum displacement in E_{corr} value was 45 mV towards cathodic region, which indicates that all studied (MAD) and (BAD) derivatives are mixed- type (anodic/cathodic) inhibitors [66-68] in 2.0 M HNO_3, cause anodic and cathodic overpotential and inhibit both the hydrogen evolution and anodic dissolution processes. The inhibitors act mainly as cathodic type in 2.0 M NaOH as seen in Fig.5 (b), whereas the maximum displacement in E_{corr} value was 129 mV towards cathodic region. The cathodic reduction of the passive film on iron in 2.0 M NaOH results in the formation of a non reducible porous layer. The surface layer was found to grow also during cathodic polarization; actually the cathodically polarized surface can be covered with Fe $(OH)_2$, as given previously in equations (10-12). Results indicate that, the cathodic reaction is the rate-determining step and all the investigated additives predominantly under cathodic control and act mainly as cathodic inhibitors from the blocking adsorption type. The magnitude of the displacement of Tafel plots is proportional to the inhibitor concentration. The inhibition efficiency strongly depends on the structure and chemical properties of the layers formed at the electrode surface under prevailing experimental conditions. Increase in

ISSN 1466-8858 Volume 15, Preprint 44 submitted 28 November 2012

inhibition efficiencies with the increase of concentrations of studied (MAD) and (BAD) derivatives shows that the inhibition actions are due to its adsorption on iron surface [69,70]. The increase in the inhibition efficiencies of iron, in 2.0 M HNO_3 solution, with increasing additive concentration can be explained on the basis of additive adsorption. The higher inhibition efficiencies values for additives in 2.0 M HNO_3 with respect to NaOH is due to the less negative potential of iron in acid solution, favoring adsorption of the additive on the metal electrode surface. The sequence of % In obtained from the polarization measurements are as follows:

α-naphthyl- ligand > β-naphthyl > *p*-anis dine > *p*-toluidine > *o*-toluidine > *m*-toluidine derivative.

The inhibition efficiencies calculated from potentiostatic polarization curves are in good agreement with those obtained from weight loss and thermometric measurements as shown in Table 3. This agreement confirms the validity of the present chemical and electrochemical measurements also support the explanation given for the effect of chemical composition on the inhibitive action of the tested synthesized (MAD) and (BAD) derivatives. Nevertheless, they showed small differences in their absolute (% In) values, could be attributed to the different experimental conditions under which each technique was carryout.

3.4. Adsorption isotherm and thermodynamic consideration

Generally speaking, corrosion inhibitors are found to protect iron corrosion in acid and alkaline solutions by adsorbing themselves on iron surface. Moreover, the adsorption process depends on the molecule's chemical composition, the temperature and the electrochemical potentials at the metal/solution interface.

ISSN-1466-8858 Volume 15, Preprint 44 submitted 28 November 2012

The adsorption isotherms describe the behaviour of the inhibitor molecules and provide information about the interaction of the inhibitor molecules with the electrode surface [71-73]. The adsorption of inhibitors at the metal-solution interface is represented as a substitution adsorption process between the inhibitor molecules ($Inh_{(sol)}$) and the water molecules on metallic surface (H_2O_{ads}):

$$Inh_{(sol)} + xH_2O_{ads} \rightarrow Inh_{(ads)} + H_2O_{sol} \quad (18)$$

Where $Inh_{(sol)}$ and $Inh_{(ads)}$ are the inhibitor species dissolved in the aqueous solution and adsorbed onto the metallic surface, respectively. $H_2O_{(ads)}$ is the water molecules adsorbed on the metal surface and x is the ratio which represents the number of water molecules replaced by a single inhibitor molecule. Fitting of the gravimetric measurement data describes the mode of interaction occurred between the inhibitor molecules and the metal surface. Adsorption is a separation process involving two phases between which certain components can be described by two main types of interaction [74]: (1) physisorption which involves electrostatic forces between ionic charges at the metal/solution interface. The heat of adsorption is low and therefore this type of adsorption is stable only at relatively low temperatures and; (2) chemisorptions which involves charge sharing or charge transfer from the inhibitor molecules to the metal surface to form a coordinate type bond. In fact electron transfer is typically for transition metals having vacant low-energy electron orbital. Chemisorptions is typified by much stronger adsorption energy than physical adsorption. Such a bond is therefore more stable at higher temperatures.

Basic information on the adsorption of inhibitor on metal surfaces can be provided by adsorption isotherm. Attempts were made to fit experimental data to various isotherms including Frumkin, Langmuir, Temkin, Freundlich, Bockris-Swinkels and Flory-Huggins isotherms. All these isotherms are of the general

form [75]:

$$f(\theta, x)\, exp(-2\alpha\theta) = K_{ads}\, C \qquad (19)$$

where $f(\theta,x)$ is the configurational factor which depends on the physical mode and the assumptions underlying the derivation of the isotherm, θ the degree of surface coverage, C the inhibitor concentration, x the size factor ratio, α the molecular interaction parameter, and K_{ads} the equilibrium constant of the inhibitor adsorption process. In this study, correlation coefficient (R^2) was used to determine the best fit isotherm which was obtained from Frumkin adsorption isotherm. According to this isotherm, θ is related to the inhibitor concentration by the following equation [76]:

$$exp\,(-2\alpha\theta) = K_{ads}C \qquad (20)$$

where the molecular interaction parameter α can have both positive and negative values. Positive values of α indicates attraction forces between the adsorbed molecules while negative values indicate repulsive forces between the adsorbed molecules [76]. Upon rearrangement of Eq. (20), the following equation is obtained:

$$\theta = [1/\,(-2\alpha)]\,\ln\,(K_{ads}C) \qquad (21)$$

If the parameter f is defined as:

$$f = -\,2\alpha \qquad (22)$$

where f is the heterogeneous factor of the metal surface describing the molecular interactions in the adsorption layer and the heterogeneity of the metal surface. Eq. (22) clearly shows that the sign between f and α is reverse, that is, if $\alpha < 0$, then $f > 0$; if $\alpha > 0$, then $f < 0$. Accordingly, if $f > 0$, mutual repulsion of molecules occurs and if $f < 0$ attraction takes place. If Eq. (22) is substituted into Eq. (21), then the Frumkin isotherm equation [77] has the following form:

$\theta = (1/f) \ln (K_{ads}C)$ (23)

where θ is the degree of surface coverage, and could be calculated by the following relationship [78]:

$\theta = \% In/100$ (24)

Eq. (23) can be transformed into:

$\theta = (1/f) \ln K_{ads} + (1/f) \ln C$ (25)

Eq. (25) is a different form of the Frumkin isotherm. The plot of θ versus ln$C$ gives a S-shaped graph, suggest that the adsorption of the investigated synthesized (MAD) and (BAD) derivatives on the iron obeyed the Frumkin adsorption isotherm. Straight lines of C_{Inh}/θ versus C_{Inh} plots indicate that the adsorption of the inhibitor molecules on the metal surface obeyed Frumkin adsorption model (Fig.6). This isotherm can be represented as:

$C_{Inh}/\theta = 1/K_{ads} + C_{Inh}$ (26)

The strong correlation coefficients of the fitted curves are around unity ($r > 0.985$). This reveals that the inhibition tendency of the inhibitors is due to the adsorption of these synthesized molecules on the metal surface [79] (Table 4). The slopes of the C_{Inh}/θ versus C_{Inh} plots are close to ≡ 1.3 which indicates the ideal simulating and expected from Frumkin adsorption isotherm [79]. K_{ads} values were calculated from the intercepts of the straight lines on the C_{Inh}/θ axis [80]. The relatively high values of the adsorption equilibrium constant (K_{ads}) as given in Table 4, reflect the high adsorption ability of these molecules on iron surface. The value of K_{ads} is related to the standard free energy of adsorption (ΔG^{o}_{ads}) by the following Eq. (27).

$K_{ads} = (1/55.5) \, exp \, (-\Delta G^{o}_{ads}/RT)$ (27)

where R is the universal molar gas constant (kJ $mol^{-1}K^{-1}$) and T is the absolute

ISSN 1466-8858 Volume 15, Preprint 44 submitted 28 November 2012

temperature (*K*). The value of 55.5 is the molar concentration of water in solution expressed in mol L^{-1}.The calculated values of ΔG^{o}_{ads} and K_{ads} of the synthesized (MAD) and (BAD) inhibitors were listed in Table 4.The negative values of ΔG^{o}_{ads} indicating the spontaneously adsorption of these molecules on the metal surface [81] and strong interactions between inhibitor molecules and the metal surface [82]. Generally, values of ΔG^{o}_{ads} around -20 kJ mol^{-1} or lower are consistent with the electrostatic interaction between charged organic molecules and the charged metal surface (physisorption); while those around -40 kJ mol^{-1} or higher involve charge sharing or transfer from the organic molecules to the metal surface to form a co-ordinate type of bond (chemisorptions) [83-85]. The values of ΔG^{o}_{ads} for both (MAD) and (BAD) compounds on iron in 2.0 M HNO_3 and 2.0 M NaOH solutions are tabulated in Table 4, being around -20 kJ mol^{-1} indicate a physical adsorption, i.e., physisorption mechanism. In addition to electrostatic interaction, there may be some other interactions [86, 87]. The high K_{ads} and ΔG^{o}_{ads} values may be attributed to higher adsorption of the inhibitor molecules at the metal-solution interface [88]. In physisorption process, it is assumed that acid anions such as NO_3^- ions are specifically adsorbed on the metal surface, donating an excess negative charge to the metal surface. In this way, potential of zero charge becomes less negative which promotes the adsorption of inhibitors in cationic form [89].

3.5. Mode of adsorption

The mechanism of the inhibition processes of the corrosion inhibitors under consideration is mainly the adsorption one. The process of adsorption is governed by different parameters almost depend on the chemical structure of these inhibitors. The presence of nitrogen and oxygen in the organic structures

ISSN 1466-8858 Volume 15, Preprint 44 submitted 28 November 2012

makes the formation of pπ-dπ bond resulting from overlap of 3d electrons from Fe atom to the 2p half or non-completely filled orbital of the nitrogen and oxygen atoms possible, which enhances the adsorption of the compounds on the metal surface. These molecules are able to adsorb on the metal surface through N and O atoms, azo groups and aromatic rings which are electron donating groups [90]. Adsorption of the studied (MAD) and (BAD) molecules on iron surface interferes with the adsorption of the anions NO_3^- and OH^- present in acid and alkaline solutions respectively. The inhibitor molecule, also can undergo the formation of a chelae complex (Fe-inhibitor complex) with Fe^{3+} ions resulting in the corrosive media, and will be readily adsorbed or deposited on the metal surface. The inhibition efficiencies increase with increasing the inhibitor concentration, molecular weight and immersion time, whiles it decreasing with increasing temperature. It was found that, the mode of adsorption depends on the affinity of the iron metal towards the $\pi -$ electron clouds of the ring system [60]. Fe has a greater affinity towards aromatic moieties; hence it adsorbs benzene rings in a flat orientation. The better performance of (BAD) derivatives is due to high electron density and large surface area which leads to more adsorption on the iron surface, also large sized molecules can provide better surface coverage and better inhibition efficiency.

Skeletal representation of the proposed mode of adsorption of the investigated (MAD) and (BAD) inhibitors is shown by Fig. (7), which clearly indicates that the active adsorption centers. Among the compounds investigated in this study, mono-*p*-anisidine (**3**) and bis-*p*-anisidine (**9**) has been found to give the best performance. This can be explained on the basis that compound (**3**) can be chemisorbed as a tridentate surface ligand. However, the inhibitor (**9**) is adsorbed in a flat orientation through a tetra dentate form. The surface coordination is through the oxygen atoms from both the OH and OCH_3 groups which rises the possibility of transferring the unshared electron of these

ISSN 1466-8858 Volume 15, Preprint 44 submitted 28 November 2012

molecules to iron in comparison to other derivatives and therefore results in a better adsorption [91]. It was concluded that, the mode of adsorption depends on the affinity of the iron metal towards the π-electron clouds of the ring system [60]. Iron has greater affinity towards aromatic moieties were found to adsorb benzene rings in a flat orientation as shown in Fig. (7). The order arrangement of increasing the corrosion inhibition efficiency of the (MAD) and (BAD) inhibitors on iron in 2.0 M HNO_3 and 2.0 M NaOH solutions was as follows:

α-naphthyl amine (**1**) > *β*-naphthyl amine (**2**) > *p*-anisdine (**3**) > *p*-toluidine (**4**) > *o*-toluidine (**5**) > *m*-toluidine (**6**) (MAD) substituents, and:

α-naphthyl amine (**7**) > *β*-naphthyl amine (**8**) > *p*-anisdine (**9**) > *p*-toluidine (**10**) > *o*-toluidine (**11**) (BAD) derivatives.

Compounds (**1**) and (**7**) are the most efficient inhibitors of the investigated (MAD) and (BAD), respectively. This seems to be adsorbed on the iron surface through each of adsorption oxygen centers and π-electron system of the benzene rings. It was found that, substituted phenyl rings in the α-position for both mono- and bis-azo derivatives **(1)** and (**7**) increases longitudinal polarization of the π -electron clouds. Thus, the adsorbed species lie flat on the iron surface causing a higher inhibitive effect value than the others derivatives. When the phenyl rings lies in the β-position for compounds **(2), (8),** this is because transverse polarization and consequently their adsorption are relatively decreased on the metal surface. The adsorption of inhibitors **(3), (9)** depends on the three oxygen adsorption sites. Methyl (CH_3-) group is more basic than the H-atom, so its presence within the azo dyes molecule causing increasing the localization of the π-electron clouds on the Fe metal surface depending on its position as follows: p > o > m-position. Thus, compound **(4)** lie before **(5)** and the compound **(6)** comes at the end of all investigated (MAD) derivatives. Consequently, compound (**9**) lie before (**10**) and the compound (**11**) comes at

ISSN 1466-8858 Volume 15, Preprint 44 submitted 28 November 2012

the end of the studied (BAD) inhibitors.

3.6. Kinetic-thermodynamic model of the corrosion inhibition

To evaluate the kinetic parameters and correlate them to their corrosion inhibition mechanism, it is now of value to analyze the kinetic data obtained in the presence of the studied mono- and bis-azo dye inhibitors from the stand point of the generalized mechanistic scheme proposed by El-Awady *et al*. [92,93].The curve fitting of the data for the investigated [(MAD) (**1**-**6**)] and [(BAD) (**7**-**11**)] inhibitors on iron in 2.0 M HNO_3 and 2.0 M NaOH solutions to the kinetic-thermodynamic model (equation 28) at 303 K.

$$\theta / (1 - \theta) = K' [I]^y \quad (28)$$

or

$$\log (\theta/1- \theta) = \log K' + y \log [I] \quad (29)$$

where y is the number of inhibitors molecules [I] occupying one active site, and K' is a constant, if relationship (29) is plotted and applicable in Fig.8. As seen, satisfactory linear relation is observed for the studied synthesized azo dye compounds. Hence, the suggested model fits the obtained experimental data. The slope of such lines is the number of inhibitor molecules occupying a single active site, (y) and the intercept is the binding constant (log K'). As mentioned, $1/y$ gives the number of active sites occupied by a single organic molecule and K'^y is the equilibrium constant for the adsorption process. The binding constant (K_b) corresponding to that obtained from the known adsorption isotherms curve fitting is given by the following equation:

$$K_b = K'^{(1/y)} \quad (30)$$

Table 4 comprises the values of $1/y$ and K_b for the studied synthesized azo dye

ISSN 1466-8858 Volume 15, Preprint 44 submitted 28 November 2012

inhibitors. This Table show that the number of active sites occupied by one molecule in the case of either (MAD) and/or (BAD) compounds ($1/y \equiv 3$ - 53).

Values of $1/y$ greater than unity implies the formation of multilayer of the inhibitor molecules on the metal surface, whereas, values of $1/y$ less than unity indicates that a given inhibitor molecule will occupy more than one active site [58]. According to the proposed kinetic-thermodynamic model, the adsorption takes place via formation of multilayer of the inhibitor molecules on the iron electrode surface. The slope values do not equal unity (gradient slopes < 1), hence the adsorption of these synthesized azo dye compounds on iron surface does not obey a Langmuir adsorption isotherm [94,95]. Frumkin adsorption isotherm (equation 15) represents best fit for experimental data obtained from applying these synthesized azo dye compounds as chemical inhibitors on iron in 2.0 M HNO_3 and 2.0 M NaOH solutions. The values of K_{ads} (equilibrium constant of the inhibitor adsorption process) and (f) are tabulated in Table 4. The lateral interaction parameter (f) has negative values, this parameter is a measure of the degree of steepness of the adsorption isotherm. The adsorption equilibrium constant (K_{ads}) calculated from Frumkin equation acquires lower values than those binding constant (K_b) obtained and calculated from the kinetic-thermodynamic model. The lack of compatibility of the calculated (K_b) and experimental (K_{ads}) values may be attributed to the fact that Frumkin adsorption isotherm is only applicable to cases where one active site per inhibitor molecule is occupied. The lateral interaction parameter was introduced to treat of deviations from Langmuir ideal behavior, whereas the kinetic-thermodynamic model uses the size parameter. The values of the lateral interaction parameter ($-f$) were found to be negative and increase from ≅ 23 to 51.This denotes that, an increase in the adsorption energy takes place with the increase in the surface coverage (θ). Adsorption process is a displacement reaction involving removal of adsorbed water molecules from the electrode metal surface and their

substitution by inhibitor molecules. Thus, during adsorption, the adsorption equilibrium forms an important part in the overall free energy changes in the process of adsorption. It has been shown [96] that, the free energy change (ΔG^{o}_{ads}) increases with increase of the solvating energy of adsorbing species, which in turn increases with the size of hydrocarbon portion in the organic molecule and the number of active sites. Hence, the increase of the molecular size leads to decreased solubility, and increased adsorb ability. The large negative values of the standard free energy changes of adsorption (ΔG^{o}_{ads}), obtained for the investigated (MAD) and (BAD) compounds, indicate that the reaction is proceeding spontaneously and accompanied with a high efficient adsorption. Although, the obtained values of the binding constant (K_b) from the kinetic model and the modified equilibrium constant (K_{ads}) from Frumkin equation are incompatible, generally have large values (Table 4), mean better inhibition efficiency of the investigated synthesized (MAD) and (BAD) compounds i.e., stronger electrical interaction between the double layer existing at the phase boundary and the adsorbing molecules. In general, the equilibrium constant of adsorption (K_{ads}) was found to become higher with increasing the inhibition efficiency of the inhibitor studied as shown in Table 4.

4. Conclusions

(1) The corrosion behaviour of iron was investigated in 2.0 M HNO_3 and 2.0 M NaOH solutions with and without addition of various concentrations of synthesized mono- and bis-azo dyes, using weight loss, thermometric and electrochemical techniques.

(2) The cathodic and anodic Tafel slopes reveal that the synthesized inhibitors are mixed type (cathodic/anodic) inhibitors in nitric, act mainly as cathodic in sodium hydroxide.

(3) All measurements show that mono- and bis-azo dye inhibitors has excellent

ISSN 1466-8858 Volume 15, Preprint 44 submitted 28 November 2012

inhibition properties for the corrosion of iron in 2.0 M HNO_3 and 2.0 M NaOH at 30°C, and the inhibition efficiency is increased with increasing the concentration of the inhibitor. The three studied methods gave consistent results.

(4) The mechanism of the inhibition processes of the corrosion inhibitors under consideration is mainly the adsorption one, i.e., they are adsorptive inhibitors and their adsorption process obeys the Frumkin adsorption isotherm (θ vs. log C_{Inh}). This behavior is an agreement with the three applied methods.

(5) The inhibition efficiency depends on the number of adsorption oxygen sites (OH and OMe groups), their charge density and π-electron clouds.

(6) The higher inhibition efficiency of the azo dye additives in acidic than in alkaline media may be due to the less negative potential of Fe in HNO_3, favouring adsorption of the additive.

(7) The large values of the change in the standard free energy of adsorption (ΔG^o_{ads}), equilibrium constant (K_{ads}) and binding constant (K_b) revealed that the reactions proceed spontaneously and result in highly efficient physisorption mechanism and stronger electrical interaction between the double layer existing at the phase boundary and the adsorbing molecules. In general, the equilibrium constant of adsorption was found to become higher with increasing inhibition efficiency of the inhibitor tested.

(8) The inhibition efficiency evaluated via theoretical methods was well accorded with reported experimental ones, following the same order as: *α*-naphthyl- ligand > *β*-naphthyl > *p*-anisdine > *p*-toluidine > *o*-toluidine > *m*-toluidine derivative.

ISSN 1466-8858 Volume 15, Preprint 44 submitted 28 November 2012

References

[1] E.M. Sherif, R.M. Erasmus, J.D. Comins, Electrochim. Acta 55 (2010) 3657–3663.

[2] I.B. Obot, N.O. Obi-Egbedi, Corros. Sci. 52 (2010) 198–204.

[3] P.B. Raja, M.G. Sethuraman, a view, Mater. Lett. 62 (2008) 113–116.

[4] M. Kissi, M. Bouklah, B. Hammouti, M. Benkaddour, Appl. Surf. Sci. 252 (2006) 4190–4198.

[5] L. Tang, X. Li, G. Mu, G. Liu, L. Li, H. Liu, Y. Si, J. Mater. Sci. 41 (2006) 3063–3069.

[6] J. Cruz, R. Martinez, J. Genesca, E.G. Ochoa, J. Electroanal. Chem. 566 (2004) 111–121.

[7] M.A. Migahed, Mater. Chem. Phys. 93 (2005) 48–53.

[8] M.A. Quraishi, F.A. Ansari, J. Appl. Electrochem. 36 (2006) 309–314.

[9] M.A. Quraishi, M.Z.A. Rafiquee, N. Saxena, S. Khan, J. Corros. Sci. Eng. (2006) 10–16.

[10] M. Lebrini, M. Lagrenee, H. Vezin, L. Gengembre, F. Bentiss, Corros. Sci. 47 (2005) 485–505.

[11] Gece. Gokhan, Corrosion Science 50 (2008) 2981-2992.

[12] I.B. Obot, N.O. Obi-Egbedi, N.W. Odozi, Corros. Sci. 52 (2010) 923.

[13] I.B. Obot, N.O. Obi-Egbedi, Corros. Sci. 52 (2010) 282–285.

[14] I.B. Obot, N.O. Obi-Egbedi, Surf. Rev. Lett. 15 (6) (2008) 903–910.

[15] L.H.Madkour, U.A. Zinhome, Journal of Corrosion Science and Engineering 13 (2010).

ISSN 1466-8858 Volume 15, Preprint 44 submitted 28 November 2012

[16] F. Bentiss, M. Lebrini, M. Lagrenee, Corros. Sci. 47 (2005) 2915.

[17] F. Bentiss, F. Gassama, D. Barbry, L. Gengembre, H. Vezin, M. Lagrenee, M. Traisnel, Appl. Surf. Sci. 252 (2006) 2684.

[18] K.F. Khaled, K. Babic-Samradzija, N. Hackerman, Electrochim. Acta 50 (2005) 2515.

[19] M. Lebrini, M. Traisnel, M. Lagrenee, B. Mernari, F. Bentiss, Corros. Sci. 50 (2008) 473.

[20] L.H. Madkour, A.M. Hassanein, M.M. Gonium, S.A. Eid, Monatschefte fur Chemie Chemical Monthly 132 (2001) 245-258.

[21] A.S. El- Gaber,L.H. Madkour, A.H. El-Asklany, A.S. Fouda, Bulletin of electrochemistry, 13 (2) (1997) 62-66.

[22] L. H. Madkour, M. M. Ghoneim, Bulletin of Electrochemistry, 13 (1) (1997) 1-7.

[23] I.B. Obot, N.O. Obi-Egbedi, Colloids Surf. A Physicochem. Eng. Aspects 330 (2008) 207–212.

[24] I.B. Obot, N.O. Obi-Egbedi, S.A. Umoren, Int. J. Electrochem. Sci. 4 (2009) 863– 877.

[25] I.B. Obot, N.O. Obi-Egbedi, Corros. Sci. 52 (2010) 198–204.

[26] I.B. Obot, N.O. Obi-Egbedi, S.A. Umoren, Corros. Sci. 51 (2009) 1868–1875.

[27] I.B. Obot, Port. Electrochim. Acta 27 (5) (2009) 539–553.

[28] I.B. Obot, N.O. Obi-Egbedi, S.A. Umoren, Corros. Sci. 51 (2009) 276–282.

[29] I.B. Obot, N.O. Obi-Egbedi, Corros. Sci. 52 (2010) 657–660.

[30] E.E. Ebenso, H. Alemu, S.A. Umoren, I.B. Obot, Int. J. Electrochem. Sci. 4 (2008) 1325–1339.

[31] E.E. Ebenso, Bull. Electrochem. 19 (2003) 209.

[32] N. Khalil, Electrochim. Acta 48 (2003) 2635.

[33] L.H. Madkour, R. M. Issa, I.M. El-Ghrabawy, Journal of Chemical Research : (S) (1999) 408-409, & (M) 1701-1726 .

[34] L.H. Madkour, M.A. Elmorsi, M.M. Ghoneim, Monatshefte fur Chemie, Chemical Monthly 126 (1995) 1087-1095.

[35] M. Behpour, S.M. Ghoreishi, N. Mohammadi, N. Soltani, M. Salavati-Niasari, Corros. Sci. 52 (2010) 4046-4057.

[36] N.O. Obi-Egbedi, I.B. Obot, Corros. Sci. 53 (2011) 263-275.

[37] X.H. Li, S.D. Deng, G.N. Mu, H. Fu, F.Z. Yang, Corros. Sci. 50 (2008) 420–2645.

[38] L.M. Vracar, D.M. Drazic, Corros. Sci. 44 (2002) 1669–1680.

[39] F. Z. Mylius, Metallkunde, 16 (1924) 81.

[40] A.S.Fouda, L.H. Madkour. A.A. Elshafei, A.H. Elasklany, Mat-Wiss,u.Werkstoff tech. 26 (1995) 342.

[41] M.M. El-Naggar, Corros. Sci. 49 (2007) 2226–2236.

[42] S.A. Umoren, E.E. Ebenso, Mater. Chem. Phys. 106 (2007) 387–393.

[43] M. Lebrini, F. Bentiss, H. Vezin, M. Lagrenee, Corros. Sci. 48 (2006) 1291.

[44] A.Y. Musa, A.A. Khadom, A.H. Kadhum, A.B. Mohamad, M.S. Takriff, J.

Taiwan, Ins. Chem. Eng. 41 (2010) 126–128.

[45] A.A. Khadom, A.S. Yaro, A.H. Kadum, J. Taiwan, Ins. Chem. Eng. 41 (2010) 122–125.

[46] M. Bouklah, B. Hammouti, M. Lagrenee, F. Bentiss, Corros. Sci. 48 (2006) 2831–2842.

[47] S. Chitra, K. Parameswari, C. Sivakami, A. Selvaraj, Chem. Eng. Res. Bull. 14 (2010) 1–6.

[48] Y. Zou, J. Wang, Y.Y. Zheng, Corros. Sci. 53 (2011) 208-216.

[49] M.M. Solomon, S.A. Umoren, I.I. Udosoro, A.P. Udoh, Corros. Sci. 52 (4) (2010) 1317–1325.

[50] V.B. Fainerman, S.V. Lylyk, E.V. Aksenenko, A.V. Makievski, J.T. Petkov, J. Yorke, R. Miller, Colloid Surf. A: Physicochem. Eng. Aspec. 334 (2009) 1–7.

[51] F. Bentiss, C. Jama, B. Mernari, H. El Attari, L. El Kadi, M. Lebrini, M. Traisnel, M. Lagrenee, Corros. Sci. 51 (2009) 1628–1635.

[52] O. Benali, L. Larabi, M. Traisnel, L. Gengembra, Y. Harek, Appl. Surf. Sci. 253 (2007) 6130–6137.

[53] F. Bentiss, M. Lebrini, M. Lagrenee, Corros. Sci. 47 (2005) 2915–2931.

[54] N.A. Negm, A.M. El Sabagh, M.A. Migahed, H.M. Abdel Bary, H.M. El Din, Corros. Sci. 52 (2010) 2122–2132.

[55] O.K. Abiola, J.O.E. Otaigbe, Corros. Sci., (2009), doi:10.1016/j.corsci.2009.07.006.

[56] K.C. Emregul, M. Hayvalı, Corros. Sci. 48 (2006) 797–812.

[57] M. Bouklah, B. Hammouti, M. Lagrenee, F. Bentiss, Corros. Sci. 48 (2006) 2831–2842.

[58] A.N. Frumkin, Z. Phys. Chem., 116 (1925) 466-484.

[59] K. Babic- Samardzija, K.F. Khalid, Heckerman, J. App. Surface Science, 240 (I-4) (2005) 327.

[60] S. Sankarapapavinasam, M.F. Ahmed, J. Appl. Electrochemical. 22 (1992) 390.

[61] A. El-Sayed, Denki Kagaku, 66(2) (1998) 176.

[62] K.F. Khaled, N. Hackenman, Electrochim. Acta 49 (2004) 485–495.

[63] S.A. Abd El-Maksoud, A.S. Fouda, Mater. Chem. Phys. 93 (2005) 84–90.

[64] I. Ahamad, R. Prasad, M.A. Quraishi, Corros. Sci. 52 (2010) 933.

[65] G. Avci, Colloid Surf. A: Physicochem. Eng. Aspec. 317 (2008) 730–736.

[66] G. Quartarone, L. Bonaldo, C. Tortato, Appl. Surf. Sci. 252 (2006) 8251–8257.

[67] L.R. Chauhan, G. Gunasekaran, Corros. Sci. 49 (2007) 1143–1161.

[68] M.A. Hegazy, Corros. Sci. 51 (2009) 2610–2618.

[69] A.B. da Silva, E. D'Elia, J.A. da Cunha Ponciano Gomes, Corros. Sci. 52 (2010) 788–793.

[70] E. Bayol, K. Kayakirilmaz, M. Erbil, Mater. Chem. Phys. 104 (2007) 74-79.

[71] E.A. Noor, A.H. Al-Moubaraki, Mater. Chem. Phys. 110 (2008) 145–154.

[72] F. Bentiss, C. Jama, B. Mernari, H. El Attari, L. El Kadi, M. Lebrini, M. Traisnel, M. Lagrenee, Corros. Sci. 51 (2009) 1628–1635.

[73] M.B. Valcarce, M. Vazquez, Mater. Chem. Phys. 115 (2009) 313–321.

[74] E.A. Noor, A.H. Al-Moubaraki, Mater. Chem. Phys. 110 (2008) 145–154.

[75] M. Sahin, S. Bilgic, H. Yilmaz, Appl. Surf. Sci. 195 (2002) 1–7.

[76] S.A. Umoren, O. Ogbobe, I.O. Igwe, E.E. Ebenso, Corros. Sci. 50 (2008) 1998– 2006.

[77] K.F. Khaled, Appl. Surf. Sci. 230 (2004) 307.

[78] M.M. Solomon, S.A. Umoren, I.I. Udosoro, A.P. Udoh, Corros. Sci. 52 (4) (2010) 1317–1325.

[79] W.A. Badawy, K.M. Ismail, A.M. Fathi, Electrochim. Acta 51 (2006) 4182–4189.

[80] M. Abdallah, Corros. Sci. 44 (2002) 717–728.

[81] L. Tang, X. Li, Y. Si, G. Mu, G. Liu, Mater. Chem. Phys. 95 (2006) 29–38.

[82] Z. Sibel, P. Dogan, B. Yazici, Corros. Rev. 23 (2005) 217.

[83] A.K. Singh, M.A. Quraishi, Corros. Sci. 52 (2010) 1373–1385.

[84] N. Soltani, M. Behpour, S.M. Ghoreishi, H. Naeimi, Corros. Sci. 52 (2010) 1351–1361.

[85] S.V. Ramesh, A.V. Adhikari, Corros. Sci. 50 (2008) 55.

[86] A.Y. Musa, A.A.H. Kadhum, A.B. Mohamad, A.R. Daud, M.S. Takriff, S.K. Kamarudin, Corros. Sci. 51 (2009) 2393–2399.

[87] M. Behpour, S.M. Ghoreishi, N. Soltani, M. Salavati-Niasari, M. Hamadanian, A. Gandomi, Corros. Sci. 50 (2008) 2172–2181.

ISSN 1466-8858 Volume 15, Preprint 44 submitted 28 November 2012

[88] O. Benali, L. Larabi, M. Traisnel, L. Gengembra, Y. Harek, Appl. Surf. Sci. 253 (2007) 6130–6137.

[89] E.A. Noor, A.H. Al-Moubaraki, Mater. Chem. Phys. 110 (2008) 145–154.

[90] K.C. Emregül, M. Hayvali, Corros. Sci. 48 (2006) 797–812.

[91] H.D. Leçe, K.C. Emregül, O. Atakol, Corros. Sci. 50 (2008) 1460–1468.

[92] A.A. El-Awady, B.A. Abd-El-Nabey, S.G. Aziz, M. Khalifa, H.A. Al-Ghamedy, International J.Chem. 1(4) (1990) 169.

[93] A.A. El-Awady, B.A. Abd-El-Nabey, S.G. Aziz, J. Electrochem. Soc. 139 (1992) 2149.

[94] A.S. Fouda, M.N. H.Mousa, F.I.Taha, A.I.El-Neanaa, J. Corrosion. Sci. 26 (1986) 719.

[95] I. Langmuir, J. Amer. Chem. Soc., 39 (1947).

[96] Szkarska- Smialowska , B. Dus, Corrosion, 23 (1967) 130.

JCSE The Journal of Corrosion Science and Engineering
ISSN 1466-8858 Volume 15, Preprint 44 submitted 28 November 2012

Table 1

A) Corrosion parameters obtained from weight loss measurements for iron in 2.0 M HNO_3 containing various concentrations of the synthesized mono-azo dye (MAD) inhibitors at 303 K.

Inhibitor	(**1**)		(**2**)		(**3**)		(**4**)		(**5**)		(**6**)	
C mol dm^{-3}	θ	(% In)	θ	(% In)	θ	(% In)	θ	(% In)	θ	(% In)	θ	(% In)
$5x\ 10^{-7}$	0.647	64.7	0.647	64.7	0.643	64.3	0.613	61.3	0.610	61.0	0.610	61.0
$1 x\ 10^{-6}$	0.671	67.1	0.656	65.6	0.644	64.4	0.615	61.5	0.611	61.1	0.616	61.6
$5 x\ 10^{-6}$	0.676	67.6	0.659	65.9	0.646	64.6	0.624	62.4	0.613	61.3	0.626	62.6
$1 x10^{-5}$	0.685	68.5	0.672	67.2	0.657	65.7	0.654	65.4	0.645	64.5	0.644	64.4
$5 x\ 10^{-5}$	0.746	74.6	0.733	73.3	0.729	72.9	0.720	72.0	0.711	71.1	0.711	71.1
$1 x\ 10^{-4}$	0.785	78.5	0.776	77.6	0.764	76.4	0.750	75.0	0.740	74.0	0.735	73.5

B) Corrosion parameters obtained from weight loss measurements for iron in 2.0 M HNO_3 containing various concentrations of the synthesized bis-azo dye (BAD) inhibitors at 303 K.

Inhibitor	(**7**)		(**8**)		(**9**)		(**10**)		(**11**)	
C mol dm^{-3}	θ	(% In)	θ	(% In)	θ	(% In)	θ	(% In)	θ	(% In)
$5x\ 10^{-7}$	0.644	64.4	0.634	63.4	0.631	63.1	0.621	62.1	0.601	60.1
$1 x\ 10^{-6}$	0.645	64.5	0.636	63.6	0.635	63.5	0.622	62.2	0.604	60.4
$5 x\ 10^{-6}$	0.646	64.6	0.639	63.9	0.649	64.9	0.648	64.8	0.607	60.7
$1 x10^{-5}$	0.662	66.2	0.655	65.5	0.657	65.7	0.658	65.8	0.627	62.7
$5 x\ 10^{-5}$	0.733	73.3	0.713	71.3	0.712	71.2	0.709	70.9	0.700	70.0
$1 x\ 10^{-4}$	0.800	80.0	0.789	78.9	0.767	76.7	0.762	76.2	0.748	74.8

ISSN-1466-8858 Volume 15, Preprint 44 submitted 28 November 2012

Table 2 Effect of different concentrations of (MAD) inhibitor **(1)** on the thermometric parameters of Fe in 2M HNO_3.

C mol dm^{-3}	θi/C°	θ_{max}/C°	t/min	Δt/min	log (Δt/min)	θ	RN/C° min^{-1}	% red. in RN
0	19.5	50.8	68	-----	-----	-----	0.460	---
5×10^{-7}	18.5	46.5	122	54	1.732	0.502	0.229	50.2
1×10^{-6}	18	46.0	130	62	1.792	0.532	0.215	53.2
5×10^{-6}	18	40.9	143	75	1.875	0.652	0.160	65.2
1×10^{-5}	18	39.9	145	77	1.886	0.671	0.151	67.2
5×10^{-5}	18	39.0	180	112	2.049	0.746	0.116	74.7
1×10^{-4}	18	37.4	196	128	2.107	0.786	0.098	78.7

Table 3 Comparison between the inhibition efficiency of (MAD and (BAD) derivatives in 2M HNO3 and 2M NaOH solutions as determined by weight loss, thermometric and polarization methods at (1×10^{-4} M inhibitor concentration) and 303 K.

Inhibitor	Corrosion Inhibition Efficiency (% In)					
	Weight loss		Thermometric		Polarization	
	HNO_3	NaOH	HNO_3	NaOH	HNO_3	NaOH
I_1 (MAD)	79	45	78.7	-----	77.8	58.5
I_2	78	51	77.7	------	76.4	61.4
I_3	76	43	74.8	------	75.9	50.5
I_4	75	40	74.2	------	72.1	45.1
I_5	74	38	74.0	-----	69.4	42.1
I_6	73	34	69.6	------	69.3	38.1
II_7 (BAD)	80	58	77.1	----	78.4	65.1
II_8	79	55	76.2	-----	76.6	63.1
II_9	77	54	77.3	-------	76.0	61.3
II_{10}	76	53	74.3	-------	74.6	54.1
II_{11}	75	49	73.7	------	73.1	50.1

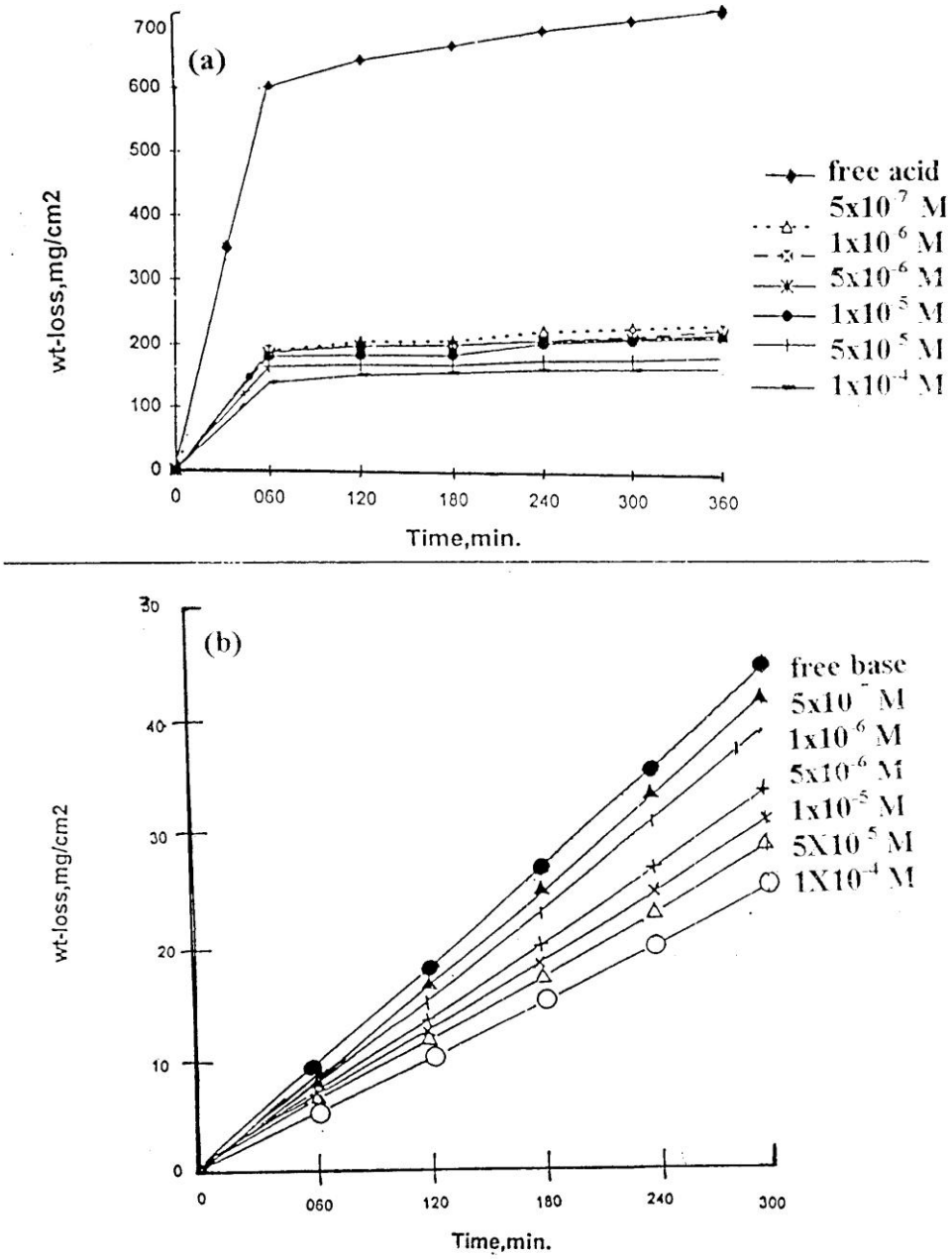

Fig.1. Weight loss vs. time curves of iron corrosion in the absence and in the presence of different concentrations of inhibitor **I(1)** in (a) 2M HNO_3 acid and (b) 2M NaOH at 303 K.

JCSE The Journal of Corrosion Science and Engineering
ISSN 1466-8858 Volume 15, Preprint 44 submitted 28 November 2012

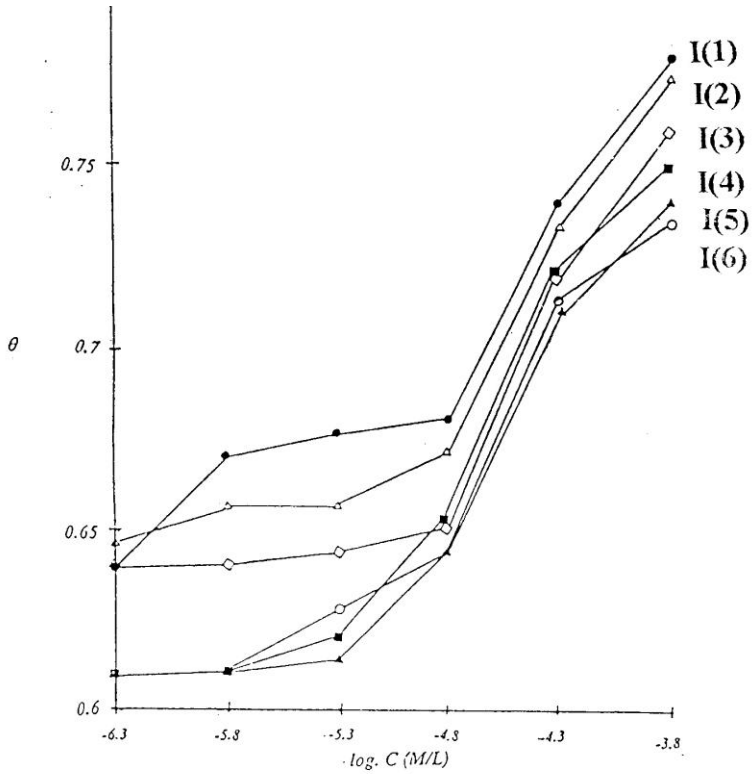

Fig.2. Variation of iron surface coverage (θ) with the logarithmic concentration of diffferent substituted azo additives in 2M HNO_3 acid at 303 K .

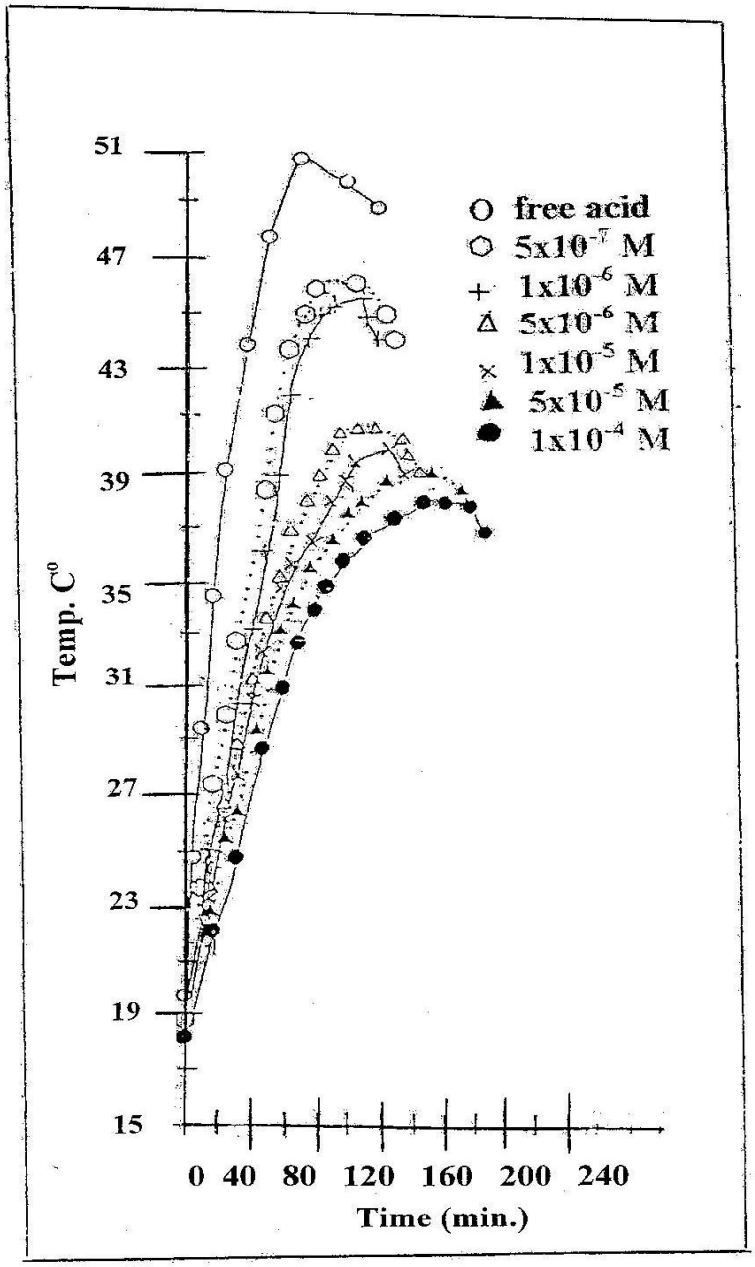

Fig.3. Temperature vs. time curves of iron corrosion in 2M HNO_3 in presence of different concentrations of (MAD) inhibitor (1).

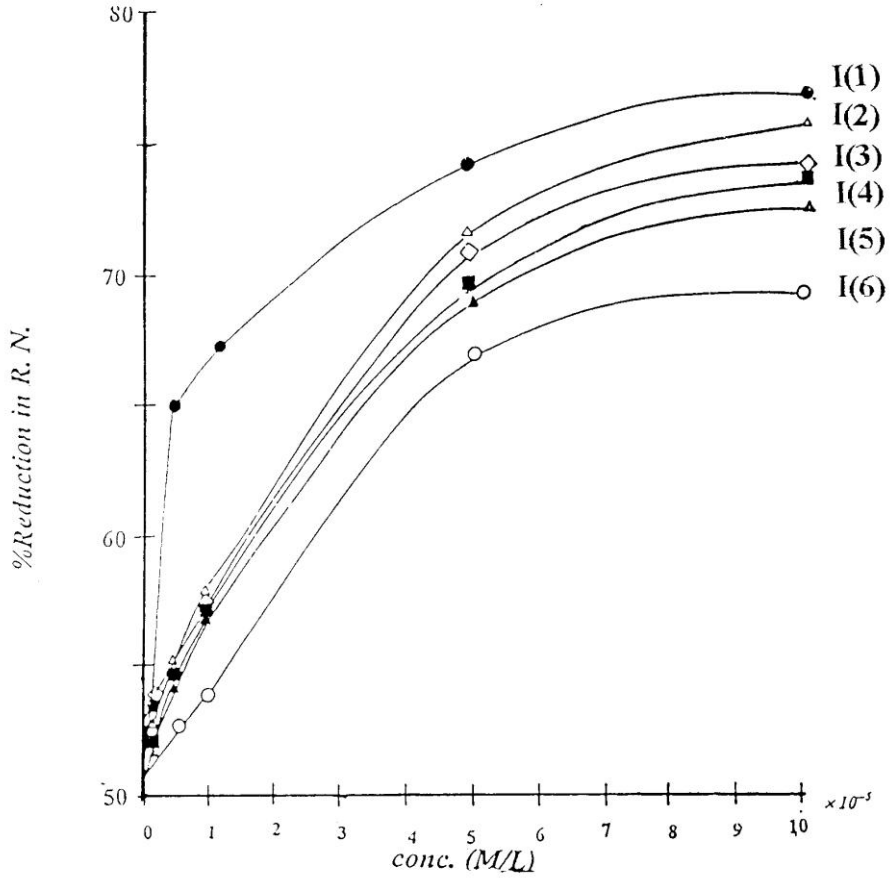

Fig.4. Effect of substituted azo derivatives concentration on percentage reduction in reaction number (% red. in RN) of iron corrosion in 2M HNO_3 acid .

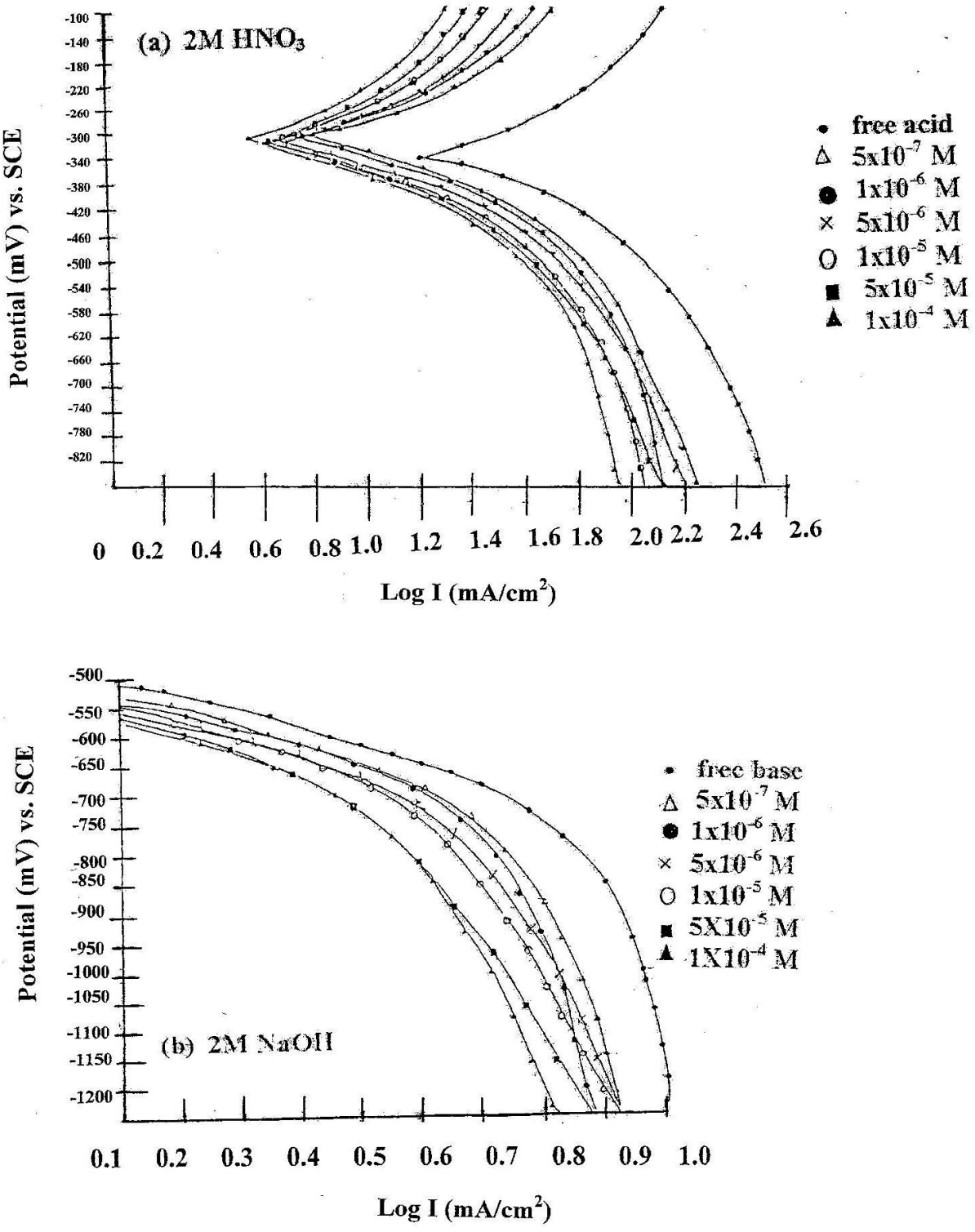

Fig.5. Polarization curve of iron corrosion in presence of different concentrations of (MAD) inhibitor (**1**) in (a) 2 M HNO_3 and (b) 2M NaOH at 30 C°.

JCSE The Journal of Corrosion Science and Engineering
ISSN 1466-8858 Volume 15, Preprint 44 submitted 28 November 2012

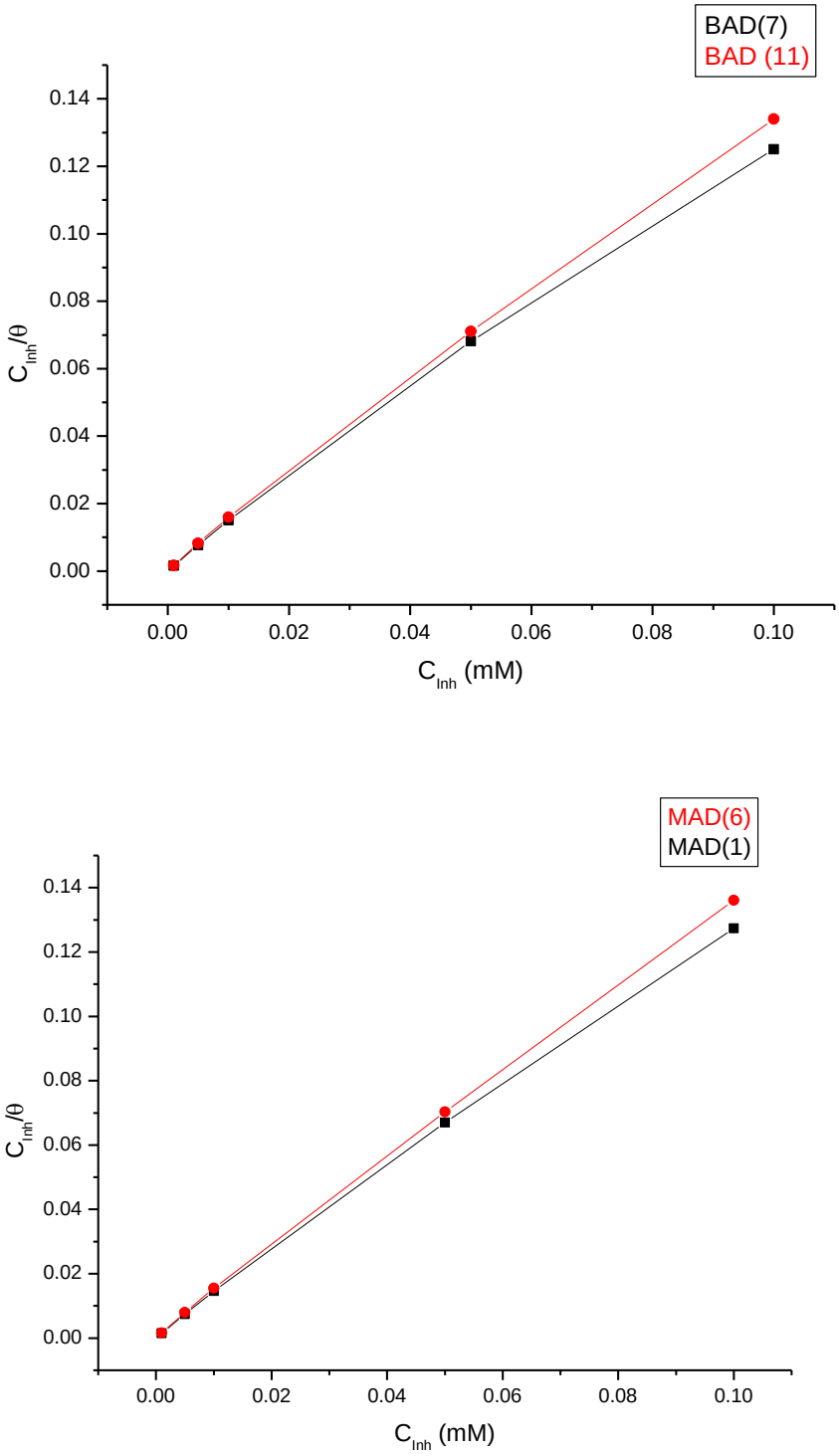

Fig. 6. Relation between C_{Inh} and C_{Inh}/θ of the synthesized bis-azo dye (**7**), (**11**) and mono-azo dye (**1**), (**6**) for iron in 2.0 M HNO_3 at 30°C.

JCSE The Journal of Corrosion Science and Engineering
ISSN 1466-8858 Volume 15, Preprint 44 submitted 28 November 2012

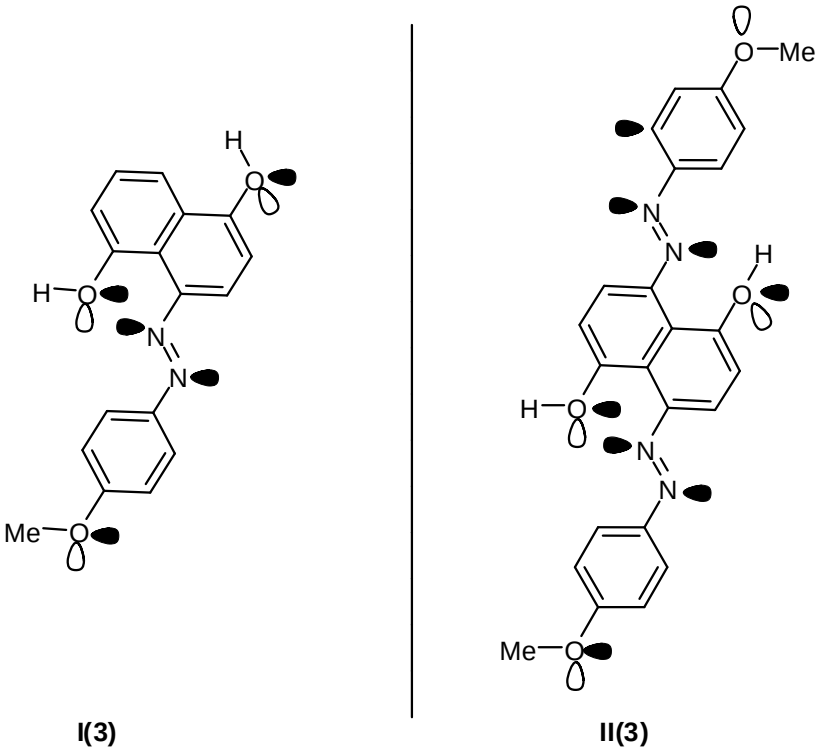

Fig.7. **Skeletal** representation of the proposed mode of adsorption of mono-*p*-anisidine (**3**) and bis-*p*-anisidine (**9**).

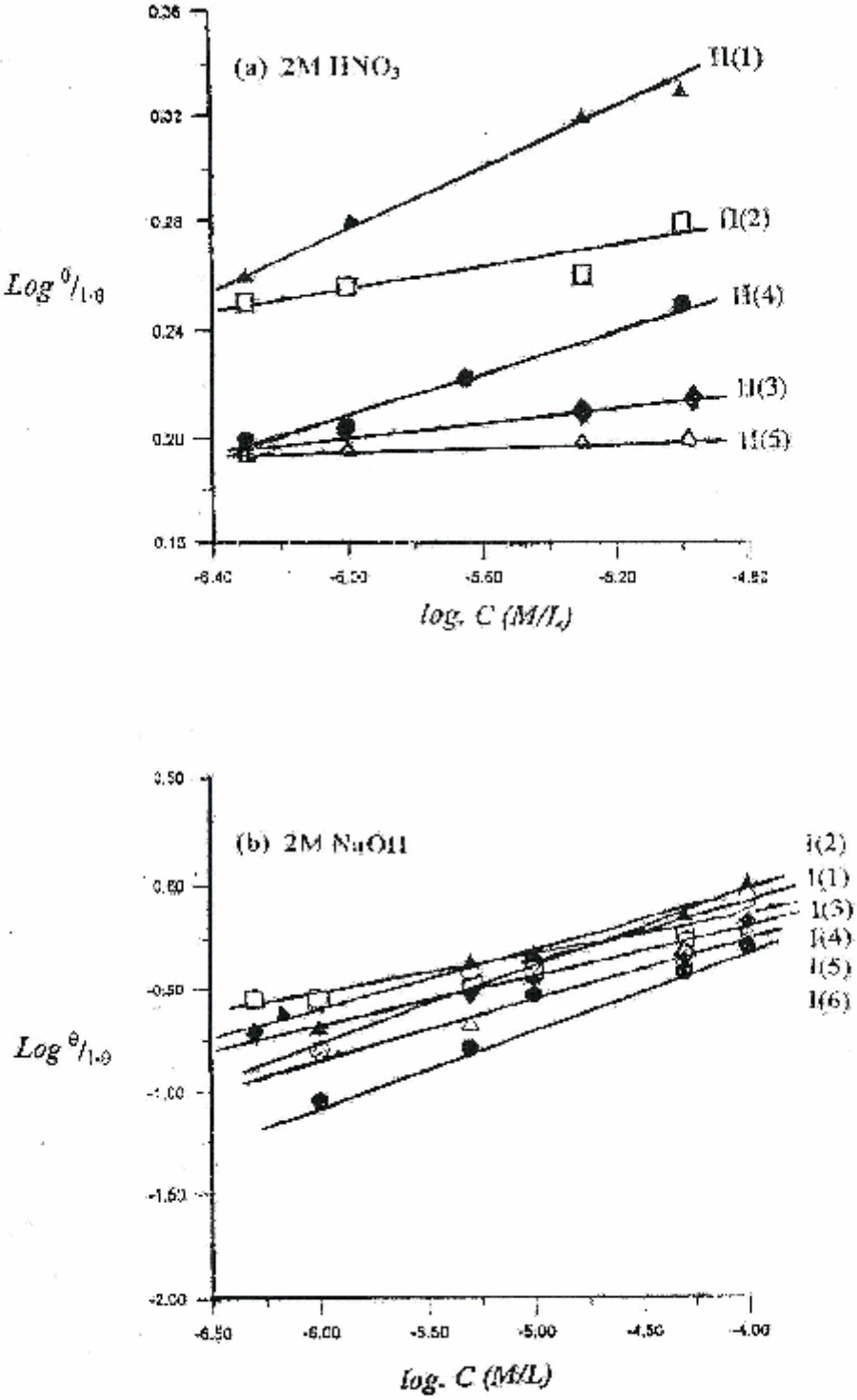

Fig.8. Application of kinetic-thermodynamic model on mono-and bis-azo inhibitors of iron in (a) 2M HNO_3 acid and (b) 2M NaOH at 303 K .

JCSE The Journal of Corrosion Science and Engineering
ISSN 1466-8858 Volume 15, Preprint 44 submitted 28 November 2012

Figure Captions:

Fig.1. Variation of weight loss against time for iron in the presence of different concentrations of mono-*α*-naphthyl amine (**1**) in (a) 2.0 M HNO_3 and (b) 2.0 M Na OH at 303 K.

Fig.2. Variation of iron surface coverage (θ) with the logarithmic concentrations of different substituted mono-azo dye derivatives in 2.0 M HNO_3 at 303 K.

Fig.3. Temperature vs. time curves of iron corrosion in 2.0 M HNO_3 in presence of different concentrations of mono-*α*-naphthyl amine (**1**).

Fig.4. Effect of substituted mono-azo dye derivatives on percentage reduction in reaction number (% red. in *RN*) for iron corrosion in 2.0 M HNO_3.

Fig.5. Tafel polarization curves for iron obtained at 30^{o}C in (a) 2.0 M HNO_3 and (b) 2.0 M NaOH containing different concentrations of mono-*α*-naphthyl amine (**1**).

Fig. 6. Relation between C_{Inh} and C_{Inh}/θ of the synthesized bis-azo dye derivatives (**7**), (**11**) and mono-azo dye derivatives (**1**), (**6**) for iron in 2.0 M HNO_3 at 30^{o}C.

Fig.7. Skeletal representation of the proposed mode of adsorption of mono-*p*-anisidine **(3)** and bis-*p*-anisidine **(9)** on the iron surface.

Fig.8. Application of kinetic-thermodynamic model on MAD and BAD inhibitors of iron in (a) 2M HNO_3 and (b) 2M Na OH at 303 K .